THE JOURNAL OF PHYSICAL CHEMISTRY B

Article

Cite This: J. Phys. Chem. B XXXX, XXX, XXX−XXX

pubs.acs.org/JPCB

Grand Canonical Investigation of the Quasi Liquid Layer of Ice: Is It Liquid?

Ignacio Pickering,[†] Martin Paleico,[†,§] Yamila A. Perez Sirkin,[†] Damian A. Scherlis,[†] and Matías H. Factorovich*[,†,‡]

[†]Departamento de Química Inorgánica, Analítica y Química Física/INQUIMAE, Facultad de Ciencias Exactas y Naturales, Universidad de Buenos Aires, Ciudad Universitaria, Pab. II, Buenos Aires C1428EHA, Argentina

[‡]Departamento de Física de la Materia Condensada, Centro Atómico Constituyentes, Comisión Nacional de Energía Atómica, Av. General Paz 1499, San Martin, 1650 Buenos Aires, Argentina

ABSTRACT: In this study, the solid−vapor equilibrium and the quasi liquid layer (QLL) of ice Ih exposing the basal and primary prismatic faces were explored by means of grand canonical molecular dynamics simulations with the monatomic mW potential. For this model, the solid−vapor equilibrium was found to follow the Clausius−Clapeyron relation in the range examined, from 250 to 270 K, with a ΔH_{sub} of 50 kJ/mol in excellent agreement with the experimental value. The phase diagram of the mW model was constructed for the low pressure region around the triple point. The analysis of the crystallization dynamics during condensation and evaporation revealed that, for the basal face, both processes are highly activated, and in particular cubic ice is formed during condensation, producing stacking-disordered ice. The basal and primary prismatic surfaces of ice Ih were investigated at different temperatures and at their corresponding equilibrium vapor pressures. Our results show that the region known as QLL can be interpreted as the outermost layers of the solid where a partial melting takes place. Solid islands in the nanometer length scale are surrounded by interconnected liquid areas, generating a bidimensional nanophase segregation that spans throughout the entire width of the outermost layer even at 250 K. Two approaches were adopted to quantify the QLL and discussed in light of their ability to reflect this nanophase segregation phenomena. Our results in the μVT ensemble were compared with NPT and NVT simulations for two system sizes. No significant differences were found between the results as a consequence of model system size or of the working ensemble. Nevertheless, certain advantages of performing μVT simulations in order to reproduce the experimental situation are highlighted. On the one hand, the QLL thickness measured out of equilibrium might be affected because of crystallization being slower than condensation. On the other, preliminary simulations of AFM indentation experiments show that the tip can induce capillary condensation over the ice surface, enlarging the apparent QLL.

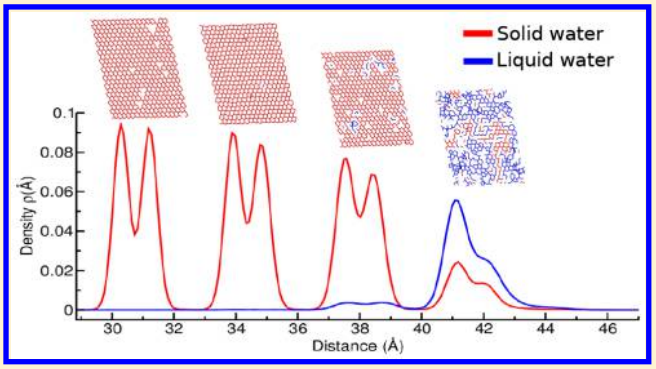

INTRODUCTION

Solid−gas interfaces are characterized by a unique phenomenon where a liquid like layer, known as quasi liquid layer (QLL), forms between both phases. This behavior was first described by Faraday in 1850 to interpret the regelation phenomena in water. Although it had been predicted more than a 150 years ago, it was only in the last two decades of the past century that surface characterization techniques achieved the nanometer scale resolution necessary to study the QLL. Since then, it has been investigated through multiple strategies, some of them being X-ray scattering,[1] atomic force microscopy (AFM),[2] proton scattering,[3] ellipsometry,[4] optical microscopy,[5] laser confocal microscopy combined with differential interference contrast microscopy (LCM-DIM),[6] attenuated total reflection in the IR (ATR-IR),[7] photoelectron spectroscopy,[8] and sum-frequency generation (SFG) spectroscopy,[9] among others.

The information gathered along the years has confirmed Faraday's prediction in a qualitative way. Nevertheless, no quantitative consensus can be achieved in two fundamental aspects: the onset temperature for surface melting, and the thickness of the QLL (δ_{QLL}) as a function of temperature. There is even less information on other important properties, such as the density of the QLL, its viscosity, hydrogen bond strength, or its ionic and electric conductivity.[10] Experimental results regarding the thickness of the QLL at different temperatures have been compiled by several authors. The information is usually presented in terms of the thickness versus temperature with respect to the triple point ($T - T_t$). We refer the interested readers to refs 10−12 to see the compiled data. A first glance to this data reveals an unsettling situation: the experimental results span over almost 2 orders of magnitude, from 1 to 100 nm, with a clear dependence on the applied

Received: January 23, 2018
Revised: April 13, 2018
Published: April 16, 2018

DOI: 10.1021/acs.jpcb.8b00784
J. Phys. Chem. B XXXX, XXX, XXX−XXX

technique and the measurement temperature. For example, 1 K bellow the melting point of water, QLL depths of approximately 100 and 15 nm have been reported based on proton backscattering and AFM measurements, respectively.[10] These differences are significant in a range of 10 K underneath the melting point; below that window, the available data starts to converge to a QLL thickness in the order of 1 nm.

The reason for these discrepancies can be ascribed to various factors. The estimation of the QLL width is often performed indirectly through the measurement of different physical properties that may have consequences on the final result.[10] Sample preparation is also of key importance. Solid water has a variety of allotropic phases. At ambient pressure or below, two can be obtained: hexagonal ice (Ih), which is thermodynamically the most stable, or stacking-disordered ice, in which layers of ice Ih and cubic ice (Ic) are found intercalated. The formation of stacking-disordered ice containing a high proportion of ice Ic is kinetically favored in small samples at low temperatures, but this phase quickly reverts to pure ice Ih above 260 K.[13] Furthermore, Ih can expose different faces: prismatic, which can be primary or secondary, and basal.[1,14] Because of a difference in the free energies of both phases (Ih versus Ic) and in the surface tension of the particular plane cut exposed (prismatic versus basal), one cannot expect to have the same QLL depth for any ice sample. Most experimental measurements do not deal with this matter and their outcome may be the consequence of mixtures of Ih and Ic and their corresponding faces, making it difficult to reproduce or to compare results from different experiments. Another important factor to take into account is the pressure and temperature control: an error of just 10% around the targeted equilibrium pressure leads to condensation (at oversaturation) or sublimation (at undersaturation) of water at rates of μm per second.[1]

Given the QLL length scale, the difficulty in getting monocrystal ice samples with a specific cut, and the challenge to compare results from different experiments, molecular simulations arise as a useful tool to get molecular insight on the QLL properties and to help in the interpretation and rationalization of the experimental data. In his pioneering work, Kroes[15] identified the existence of a quasi liquid layer at the ice surface employing classical molecular dynamics with the TIP4P water model in the NVT (constant number of particles, volume and temperature) ensemble. Since then, much effort has been invested to reproduce experimental results with simulations. A decade ago, Conde et al. performed NVT simulations of thousands of particles in which the liquid layer was identified by means of a tetrahedral order parameter (q).[16] These authors compared the QLL depths of the basal, primary prismatic, and secondary prismatic faces for the TIP4P/ice model, which fits the temperature of solidification. For all temperatures they found the following relation: $\delta_{QLL}^{basal} > \delta_{QLL}^{primary} > \delta_{QLL}^{secondary}$. In particular, for 270 K they reported the values 7.5 Å (basal), 6.8 Å (primary), and 4.4 Å (secondary). In turn, the QLL depth of the secondary prismatic face was examined with different water models, finding for all studied temperatures $\delta_{QLL}^{TIP4P/2005} > \delta_{QLL}^{TIP4P} > \delta_{QLL}^{SPC/E}$. At 270 K the thicknesses were 6.0 (TIP4P/2005), 4.6 (TIP4P), and 4.0 Å (SPC/E). In another study dating from the same year, path integral molecular dynamics simulations were conducted in order to account for possible quantum effects at the solid−vapor interface,[17] with results similar to those obtained from the classical simulations. More recently coarse grained models have been applied to study the QLL of water, in particular in the basal face. Limmer et al.[18] used capillary wave theory in combination with local order parameters to identify the liquid layer over the ice surface in NVT simulations at 3 K below the melting point, for time scales up to 1 μs, and exposed surfaces as large as 130 × 130 Å^2, with which they found a QLL depth of 7 Å. Shepherd and collaborators explored the QLL with the mW model[19] in simulations extended up to 1.3 μs, using a slab model consisting of 21 000 molecules and an exposed interface of 70 × 86 Å^2. The sampling was carried out in the NVT ensemble, after stabilizing the slab exposing solid−vacuum interfaces with lateral pressures of methane of 150 atm. The CHILL algorithm was used to identify liquid water. Applying this scheme, they found an average size of 5 Å for the QLL, with large fluctuations reaching 2 nm spanning around 50 ns. In a recent work by Hudait et al.,[20] molecular dynamics were performed with the mW model in the NVT ensemble to study ice Ih exposing the basal face, in order to understand the effects of ions and organics on the properties of the ice surface. Simulations were run at 260 K both in the presence and in the absence of solutes, for a slab of area 100 nm^2 and time-windows of 1 μs, employing the CHILL+ algorithm[21] to identify liquid water at the surface. The authors found, for pure water, that the external layers could be described in terms of ice islands surrounded by liquid, which covered nearly 40% of the surface.[20]

In general, these results show consistency between simulations and water models, whether quantum or classical, reporting QLL depths of at most 1 nm. Nevertheless, these estimations are about 1 order of magnitude below most experiments. In recent work, Gelman and co-workers[11,22] sought to reproduce the experimental conditions in AFM measurements of the QLL, by performing classical molecular dynamics simulations of nanoindentation of an ice slab. Two criteria were employed to identify water belonging to a liquid environment: (i) the time average of the number of hydrogen bonds and (ii) the tetrahedral order parameter q. Among other findings, they observed that the tip induced melting as it penetrated the ice.

In the present work, we aim at taking into account the pressure conditions at which most experiments are carried out. Hence, we performed grand-canonical molecular dynamics (GCMD) simulations for solid water slabs, to explicitly consider the vapor−solid equilibrium. The monatomic mW water model[23] was used, which has a proven performance both in the study of solid−liquid[21,24−26] and liquid−vapor[27−30] equilibria. First, we characterize the solid−vapor equilibrium of the mW model, including its vapor pressure as a function of temperature, and the vaporization enthalpy, analyzing as well certain aspects of the evaporation and nucleation dynamics. Next, we focus on the characterization of the QLL in the grand canonical ensemble, comparing with the results in other ensembles and examining the effect of the size of the exposed interface. Then, we study the QLL below and above the equilibrium pressure and present preliminary results of μVT simulations that mimic an AFM experiment. We finally discuss the advantages of performing simulations in the grand canonical ensemble to approach real experimental conditions.

METHODOLOGY

Water Model. Water is described by the monatomic mW model,[23] which lacks electrostatic interactions and is based on the short-range Stillinger−Weber (SW) potential, consisting of a sum of two-body attraction terms and three-body repulsion

DOI: 10.1021/acs.jpcb.8b00784
J. Phys. Chem. B XXXX, XXX, XXX−XXX

terms.[31] Although hydrogen atoms are not explicitly represented, it faithfully describes hydrogen bonding thanks to the three-body contribution that encourages specific angle configurations through an energetic penalty. The mW model reproduces the energetics, density, and structure of liquid and solid water and its phase transitions, with comparable or better accuracy than most atomistic models, at nearly 1% of the computational cost.[23] In recent years it has been repeatedly applied to study the solid−liquid[21,24−26] and liquid−vapor[27−30] equilibria.

The vapor pressure of mW liquid water, 0.5 mbar at room temperature, is nearly 2 orders of magnitude below the experimental value.[28] We have shown that this shift can be accurately predicted via a statistical thermodynamics analysis, having its origin in the lack of rotational entropy of the mW model in the gas phase.[28] In spite of this shift, the liquid−vapor behavior of experimental water is rigorously reproduced by the mW potential in terms of relative vapor pressure (P_v/P_v^*), as it has been assessed for the dependence of equilibrium pressure with respect to temperature,[28] size of liquid droplets,[29,32] confinement,[30] and electrolyte concentration.[27]

Molecular Simulations. Classical molecular dynamics were performed with the open-source simulation program LAMMPS[33] in three ensembles: (i) at constant number of particles, volume and temperature (NVT), or canonical ensemble; (ii) at isobaric−isothermal conditions with constant number of particles (NPT); and (iii) at constant chemical potential, volume and temperature (μVT), also called the grand canonical ensemble. Grand canonical molecular dynamics schemes reproduce the temporal evolution at a controlled chemical potential, allowing for the exchange of water particles between the simulations box and a reservoir. The equations of motion were integrated using the Verlet algorithm with a time step of 5 fs. The temperature of the system was controlled with the Nosé−Hoover thermostat with a relaxation time of 1.25 ps. Periodic boundary conditions were used in all directions.

Slabs exposing the basal and the primary prismatic (hereafter called prismatic) faces normal to the z axis were studied in each of the three ensembles. For each face, two system sizes were analyzed. To analyze certain features, an additional model of much larger dimensions and exposing the basal face was employed. The characteristics of the different models investigated are summarized in Table 1.

Table 1. Summary of Model Systems Characteristics[a]

name	molecules	slab dimensions (nm)	area exposed (nm^2)
HBs	768 000	26.4 × 30.5 × 29.4	800
BBs	20 736	8.0 × 9.0 × 9.0	72
BPr	27 648	8.0 × 9.0 × 12.0	72
SBs	768	2.6 × 3.0 × 3.0	7.8
SPr	768	2.6 × 3.0 × 3.0	7.8

[a]In the acronym, B accounts for big box, S for small box, H for huge box and Bs and Pr denote basal and prismatic respectively.

The nomenclature goes as follows: B stands for big box, S for small box, H for huge box, Bs and Pr mean basal and prismatic, respectively, and the simulation ensemble will be given between parentheses. The dimensions showed in the third column correspond to the slab. The simulation cell includes 15 Å of vacuum for the small box, 50 Å for the big box, and 100 Å for the huge one, which are beyond the cutoff of the potential, of approximately 5 Å.[23] The proportions between the three slab dimensions are approximately preserved along the different systems, to mimic the bulk QLL without introducing instability effects that may arise from large x to z or y to z ratios.[18,34]

Determination of Vapor Pressures. The vapor pressure was computed using the Grand Canonical Screening (GCS) scheme.[28,29] This method requires various grand canonical simulations to be performed in the presence of a solid−vapor (or liquid−vapor) interface, each one at a different chemical potential around the presumed equilibrium value μ_{eq}. If the chemical potential μ fixed in the simulation is above μ_{eq}, the number of molecules increases until the simulation box fills completely. Conversely, if μ is below μ_{eq} at the beginning of the simulation, the number of molecules decreases until all particles have disappeared. By repeating this computational experiment for a given system at different chemical potentials, upper and lower bounds can be established for μ_{eq}, which is directly linked to P_v.[28,29]

Characterization of the QLL and of Its Depth. The particles corresponding to the QLL were identified with the help of the CHILL+ algorithm,[21] which, by means of an order parameter criterion, allows for the classification of liquid, Ih, and Ic. This analysis made it possible to determine the percentage of liquid water (%LW) contributing to the density distribution profiles as a function of z (the direction normal to the interface), which were in turn obtained by integrating the number of particles on the xy plane for each z throughout the simulation time. After the identification of liquid water, we adopted two different approaches to estimate the thickness of the QLL (δ_{QLL}):

Molecule Counting (MolC). A usual practice to calculate the QLL width is through the density definition[16]

$$\rho = \frac{N_{QLL}}{L_x L_y \delta_{QLL}} \Rightarrow \delta_{QLL} = \frac{N_{QLL}}{L_x L_y \rho} \quad (1)$$

where N_{QLL} is the number of liquid molecules, ρ is the number density for liquid water, and L_x and L_y are the slab dimensions parallel to the interface. Thus, this method assumes that the density of the QLL is the same as that of the liquid. For ρ we use the equilibrium mW density at 298 K.

Density Profile Integration (DI). Alternatively, to avoid the use of eq 1, it is possible to define δ_{QLL} as the stretch of slab that contains the liquid. Due to fluctuations, a tiny number of liquid particles may be detected even well below the surface deep in the solid phase, and therefore, to put the DI idea into practice, it is necessary to define a certain percentage of liquid water to be enclosed within the QLL. We choose here to compute δ_{QLL} as the region that encloses 95% of the liquid water, and so the QLL is obtained by the integration of the liquid density profiles, from 2.5% up to 97.5%, assigning the integration spatial range to the QLL depth.

Clearly, these two criteria to calculate δ_{QLL} suffer from some degree of arbitrariness. It is possible to conceive yet other ways to estimate the QLL thickness, but all of them will be affected by some ad hoc assumptions or arbitrary definitions. In the next section, the effect of the particular definition on the value of δ_{QLL} will be examined.

RESULTS AND DISCUSSION

Vapor Pressure, Sublimation Enthalpy, and Nucleation Dynamics of Ice Ih. In the first place, the GCS scheme was applied to characterize the sublimation equilibrium of ice Ih for the mW model. To the best of our knowledge, this portion

DOI: 10.1021/acs.jpcb.8b00784
J. Phys. Chem. B XXXX, XXX, XXX−XXX

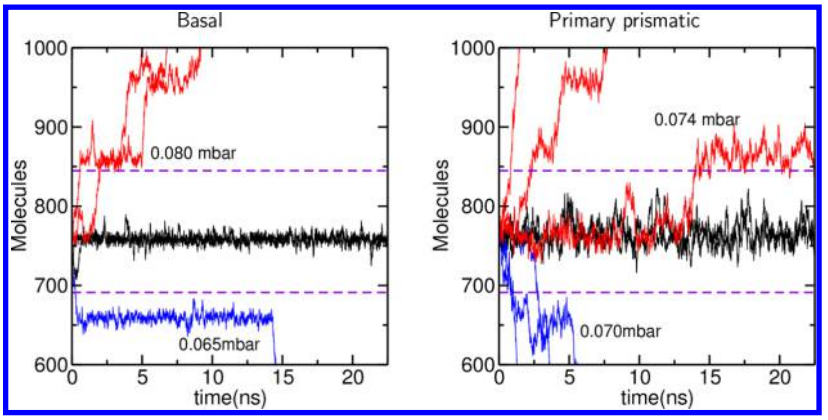

Figure 1. Evolution of the number of water particles as a function of time in GCMD simulations of an ice slab at 270 K in the small box (see Table 1). Left: basal face. Right: prismatic face. The red and blue lines identify oversaturation and undersaturation pressures, respectively. The black curves correspond to equilibrium, while the horizontal dashed violet lines mark the ±10% range around the initial number of water particles.

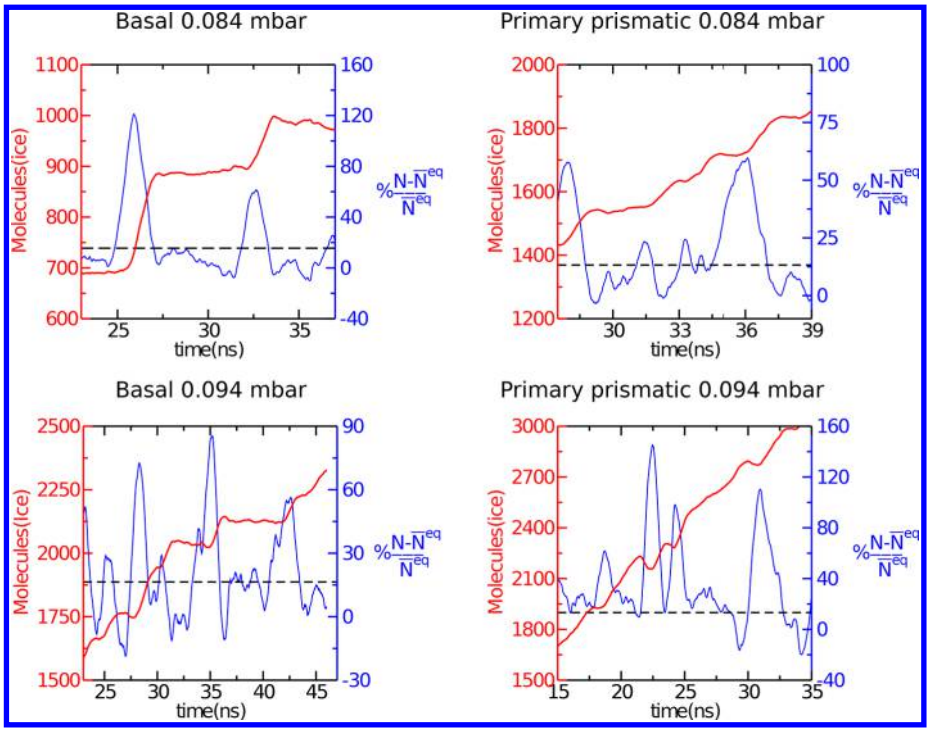

Figure 2. Number of ice molecules (red axis) and the relative deviation of the amount of liquid from its average equilibrium value (blue axis) as a function of time for the basal and prismatic faces at two oversaturation pressures and 270 K. The black dashed line marks the average plus two times the relative standard deviation. The Savitsky−Golay filter has been applied to the raw data in order to get smother curves.

of the phase diagram has not been studied for this force field. Following ref 28, the system was assumed to be at its equilibrium pressure when the number of molecules in the box remained within a range ±10% around the starting value during the simulated time, which in this case was 22.5 ns. Figure 1 shows the number of particles as a function of time for GCMD simulations of the basal and prismatic faces at various chemical potentials. These were carried out at 270 K in the small simulation cell. For the basal cut, the equilibrium pressure turned out to be 0.072 ± 0.008 mbar, whereas for the prismatic one it was 0.072 ± 0.002 mbar. Thus, no appreciable difference was found between the equilibrium pressures of these two interfaces.

Furthermore, Figure 1 reveals a distinctive condensation and evaporation dynamics, which proceeds in sudden steps. The number of water molecules changes significantly in a short time, to give rise to a metastable state in which this number remains approximately constant, until a new jump is observed. To better understand the condensation mechanism, we investigate in Figure 2, for the oversaturation pressures of 0.084 and 0.094 mbar at 270 K, the number of ice molecules and the relative deviation of the amount of liquid from its average value at equilibrium (0.072 mbar for 270 K) as a function of time. The black dashed line marks the average plus two times the relative standard deviation, indicating meaningful water accumulation. Only part of the full 45 ns dynamics is shown in each case. Different behaviors for the basal and prismatic faces are seen during condensation at the two pressures. For the basal face the appearance of new layers of ice is of a stepwise nature. At some point in the dynamics, liquid water starts to deposit on the surface way above the fluctuations observed in equilibrium conditions, as can be seen by the water uptake surpassing the

DOI: 10.1021/acs.jpcb.8b00784
J. Phys. Chem. B XXXX, XXX, XXX−XXX

dashed black line. The deposition continues until it triggers crystallization, after which a new induction stage begins. The elapsed time from the onset of massive water deposition until the beginning of the freezing cycle is in the order of 1 ns for the oversaturation pressure of 0.094 mbar. The prismatic face presents a slightly different behavior: the growth of ice is smoother and continuous and sometimes occurs without being preceded by a significant liquid accumulation, as can be seen for example at 0.094 mbar between 26 and 29 ns. This kind of growth is not seen for the basal face. Moreover, visual inspection of the dynamics suggests that crystallization in the prismatic case is often preceded, aside from the deposition from the vapor, by a significant melting of the preexisting ice layer. This is somehow reflected at 0.094 mbar in the small depressions in the red curve coincident with the peaks of liquid. These distinctive behaviors are not so manifest at 0.084 mbar, though the basal plane presents typically longer induction times.

The particular behaviors of the basal and prismatic faces can be explained in terms of their different structures. In the former, water layers must have a specific two-dimensional hydrogen bond configuration in order to solidify, which is not necessary in the case of the prismatic surface.[35] This translates into a larger activation energy for the basal face that results in longer induction times for crystallization. The appearance of cubic ice delays solidification, since it is difficult to grow more than one layer of Ic, which is not a thermodynamically stable phase, while the stacking of a new Ih layer over cubic ice is also penalized due to the different symmetry.

Consistently with the difference in activation barriers, our simulations yield a slower crystallization rate on the basal plane in comparison with the prismatic one. This observation can not be taken in strict quantitative terms, because in GCMD simulations time is distorted as a result of the Metropolis Monte Carlo moves. Even so, Figure 1 shows that, in order to achieve evaporation or crystallization on the basal surface within the time frame of 22.5 ns, the pressures have to be further apart from the equilibrium than they are in the case of the prismatic face. Also, the stepwise crystallization observed for the basal face can be understood as the consequence of a reorganization of the accumulated liquid water to reach the appropriate structure to solidify over a basal plane.

Figure 3 presents for each face three selected frames from the GCMD simulations at oversaturation conditions (270 K and 0.094 mbar) that can be helpful to visualize the mechanism taking place. Each structure corresponds to a different stage in the curves depicted in Figure 2, lower panel. For both faces, the addition of particles occurs at the QLL−vapor interface and in a liquid environment, followed by solidification of a new layer of ice. In particular, during our simulations the basal surface exhibits, from time to time, stacking of Ic during the deposition of a new layer. This behavior, which has been previously reported,[24] seems to have a kinetic origin and is supposed to reflect the natural configuration appearing during fast interfacial crystallization at low temperatures.[13,36] In both faces, the surface exhibits a full liquid coverage at the onset of the condensation process, which has been claimed to be necessary for the formation of cubic layers.[37] The emerging structure, known as stacking-disordered ice, reverts to Ih with time above 260 K according to laboratory measurements.[13]

Figure 4 shows on the left panel the vapor pressures at different temperatures, for the solid−vapor equilibria, plotted as $\ln(P/mbar)$ against $1/T$, and on the right panel a full phase

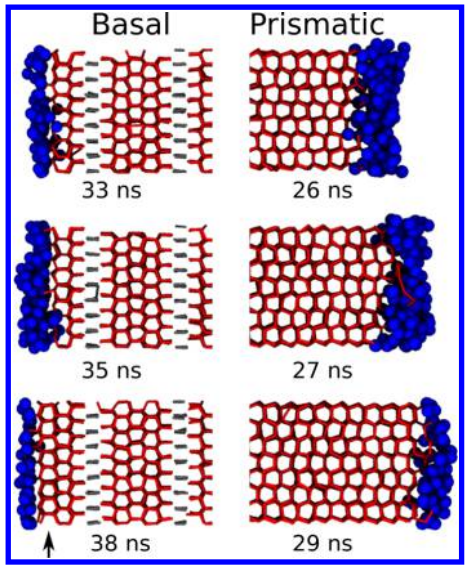

Figure 3. Sequence of snapshots corresponding to condensation at oversaturation conditions (270 K and 0.094 mbar), for the basal and prismatic planes, according to GCMD simulations. Red and gray sticks represent hexagonal and cubic ice, respectively. Blue spheres show liquid water molecules. Each frame can be identified with a particular point on the curves presented in the lower panels of Figure 2. The arrow for the basal model shows the newly formed ice layer. Only the region next to the interface is shown.

diagram for the low pressure region around the triple point. Our simulations provide a linear trend for $\ln(P/mbar)$ versus $1/T$, meaning that the Clapeyron−Clausius relation holds for both the basal and prismatic faces of mW water, for the range of temperatures studied. The enthalpy of sublimation obtained from the slope is 50 ± 2 kJ/mol for the basal plane and 50.1 ± 0.1 kJ/mol for the prismatic face. Hence, we observe no significant differences for the enthalpy of sublimation of ice Ih exposing either face.

A full phase diagram for the mW model in the low pressure region can be constructed by extrapolating previous data for the solid−liquid equilibrium at high pressure[38] and new liquid−vapor coexistence points produced for this work which extend the range reported in ref 28. The resulting diagram is shown on the right-hand side of Figure 4, where the coexistence curves between ice Ih, water vapor, and liquid water can be appreciated. The intersections between the three curves, green points in the figure, provide an estimation of the triple point for the mW model. In our case the solid−vapor (blue) and liquid−vapor (black) curves intersect at a temperature of 274.4 K and a pressure of 0.1 mbar, while the solid−liquid curve (red) intersects the other two at roughly the same temperature and pressure, 272.5 K and 0.08 mbar. From this we estimate the triple point for the mW model to be around (273 ± 1 K, 0.09 ± 0.01 mbar). It should be noted that, due to the absence of solid−liquid coexistence data at low pressures for the mW model, this curve had to be extrapolated from high-pressure data-points,[38] which makes our estimation highly approximate. Comparison between our results and the experimental phase diagram must be done in terms of relative pressures, since the absolute values given by the mW model lack the rotational contribution and are therefore shifted with respect to real water (see subsection Water Model above). The experimental vapor pressure at the triple point relative to the vapor pressure at 298.15 K is 0.2, which correlates very well

DOI: 10.1021/acs.jpcb.8b00784
J. Phys. Chem. B XXXX, XXX, XXX−XXX

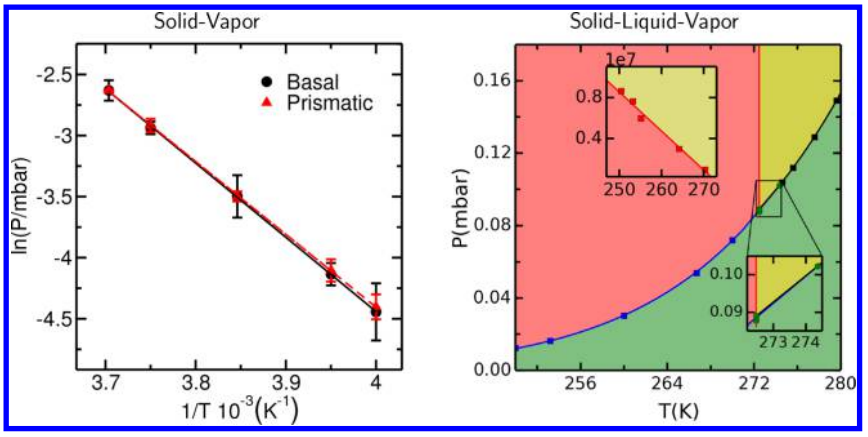

Figure 4. Left: Verification of the Clapeyron−Clausius relation for the basal (black) and prismatic (red) faces of Ih, according to the mW model. Right: Phase diagram at low pressure for the mW model. The curves indicate two-phase coexistence: blue for solid−vapor, black for liquid−vapor, and red for solid−liquid. The red curve was obtained from a linear regression considering the high pressure data of ref 38 shown in the upper inset. Green points indicate intersections between the coexistence curves. A magnification of the triple-point region is portrayed in the lower inset.

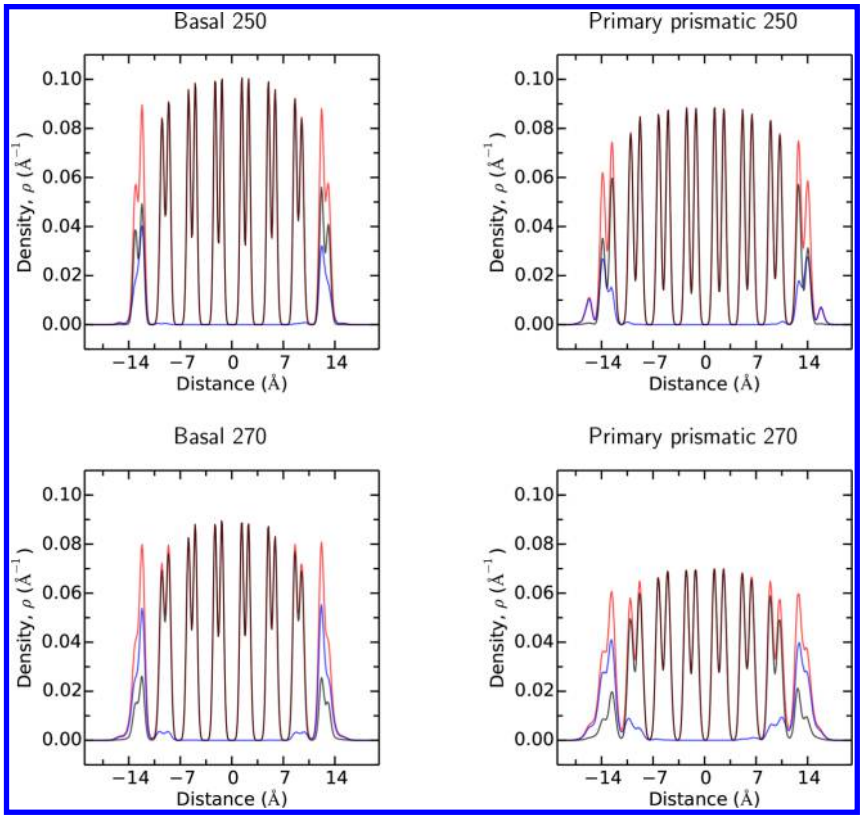

Figure 5. Density profiles for the water slab from μVT simulations in the small box at 250 and 270 K. The profiles are depicted with respect to the z direction, normal to the surface, for both the basal and prismatic planes. The red, black, and blue lines represent total, solid, and liquid water, respectively.

with the value of 0.18, which is the corresponding ratio for the mW model.[28]

The Quasi Liquid Layer. Once the equilibrium curve of P versus T for mW ice Ih has been established, it is possible to examine the QLL along this curve in the μVT ensemble, in addition to the NPT and NVT situations. First, we focus on the spatial localization of the QLL. The CHILL+ algorithm distinguishes water molecules in a liquid like environment, from those belonging to a solid, either Ih or Ic phases. The density profiles obtained from simulations of the SBs(μVT) and SPr(μVT) systems, at 250 and 270 K, are presented in Figure 5. These profiles are plotted against the z direction, normal to the exposed face. The figure shows that each water layer, also called bilayer, is split in two peaks, which reflects the fact that the molecules are organized in two parallel subplanes slightly displaced to optimize the hydrogen bond network. Every layer has a certain degree of solid and liquid particles. The liquid composition in the outermost bilayer goes from around 40% at 250 K to 70% at 270 K. Even at 250 K the molecules that are recognized as liquid contribute 40% of the total amount of water in the first layer, distributed over its entire length, which raises a question on the meaning of the

DOI: 10.1021/acs.jpcb.8b00784
J. Phys. Chem. B XXXX, XXX, XXX−XXX

QLL depth. These results portray an interface that can not be characterized as either solid or liquid, but as a combination which liquid nature increases with rising temperature. In this situation, it is not evident how to assign a depth to the QLL, not to mention the very existence of a liquid layer. Instead, its properties can be considered intermediate between those of the liquid and solid phases due to a mixture where the proportions oscillate, during the simulation time, around an equilibrium position that is a function of the temperature. Table 2 shows

Table 2. Liquid Water Content for the First and Second Layers of the Different Model Systems of Table 1, Analyzed at 270 K

name	%LW first	%LW second	name	%LW first	%LW second
SBs(NPT)	68.3	6.2	BBs(NPT)	65.5	4.5
SPr(NPT)	75.0	11.5	BPr(NPT)	74.6	11.8
SBs(NVT)	69.8	6.5	BBs(NVT)	69.3	5.7
SPr(NVT)	71.4	12.4	BPr(NVT)	75.1	14.9
SBs(μVT)	69.1	6.1	BBs(μVT)	70.8	6.4
SPr(μVT)	72.9	15.6	BPr(μVT)	74.9	14.8
HBs(μVT)	69.3	6.1			

the fraction of liquid water in the outermost layers for the different slabs and faces studied in the three ensembles. As stated in the literature, the width of the solid−vapor interface, including the width of the QLL, may be related to the magnitude of the density fluctuations at the surface. These fluctuations can be expressed in terms of capillary waves, which amplitude is dependent on the exposed surface.[18] For the model systems investigated in this work, however, there is no dependence of the QLL liquid content on system size nor significant differences between the ensembles used.

A question that may be formulated at this point is what is the structure of this solid−liquid mixture? In order to further understand the nature of the QLL, we present in Figure 6 snapshots of the two outermost bilayers for the SBs(μVT), BBs(μVT), and HBs(μVT) models.

The images in Figure 6 are complementary to the density profiles in Figure 5 to provide a complete picture of the QLL. For all three model slabs, solid regions in the first layers (depicted in red and yellow) coexist with liquid areas (in blue), reflecting a nanophase segregation at the surface. Liquid water is abundant in the first bilayer, constituting nearly a 70% at 270 K, but has a small presence in the second bilayer. This bidimensional nanophase segregation is well represented in the three models. Nevertheless, the largest slab allows for longer correlation distances, and thus, on the HBs surface, the solid nanophases develop over tens of Å surrounded by the liquid phase. The length scale of the clusterization is already visible in the BBs model, appearing converged in the HBs system, where the size of the ice clusters is well below the area of the slab. According to our simulations, the typical dimensions of these solid domains are in the order of a few nanometers. These 2D domains are likely to play a role in the crystallization process at the solid−gas interface. We note that an analogous description of the ice surface has been provided by Hudai al. in a very recent computational study at 260 K.[20]

The content of liquid in the external layers and the thickness of the QLL at different temperatures were studied in the smallest slab model and the μVT ensemble. Grand canonical simulations were performed in the temperature range from 250

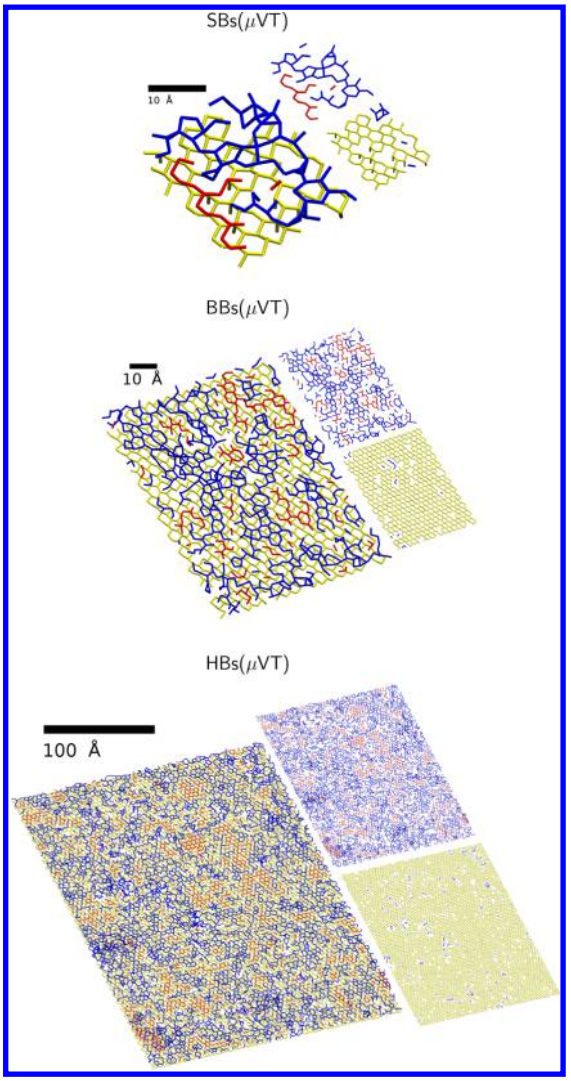

Figure 6. Snapshots of the first two bilayers of the SBs (top panel), BBs (middle panel), and HBs (bottom panel) models at 270 K. The connectivity between water molecules lying less than 3.5 Å apart is shown with sticks (this separation corresponds to the first minimum in the radial distribution function of liquid mW water[23]). In each panel, the images on the left show the first layer overlaid on the other one. On the right, the first and second layers are shown separately and in a smaller scale. The length bar corresponds to the left image. Liquid water is represented in blue, while the ice is shown in red in the first bilayer and in yellow in the second one.

to 270 K, or from 24 to 3 K below the mW melting point. The results for %LW are shown in Figure 7 along with the QLL length calculated with the DI and MolC approaches. The liquid content of the second bilayer is almost negligible below 260 K for both faces, so the major contribution to the QLL arises from the first bilayer, unless the temperature approaches 270 K. In this temperature range the liquid content in the outermost bilayer steadily increases from around 40% to 70%. These results were already apparent in the density profiles exhibited in Figure 5, where it can be seen that within each layer the liquid is distributed along the z coordinate as much as the solid.

The thicknesses obtained with the DI method reproduce the trends observed for %LW. In the crystal, the separation between prismatic layers is larger than between basal planes (see Figure 5), and this is reflected in the DI estimates for δ_{QLL}, which turn out to be 1−2 Å larger for the prismatic surface. The

DOI: 10.1021/acs.jpcb.8b00784
J. Phys. Chem. B XXXX, XXX, XXX−XXX

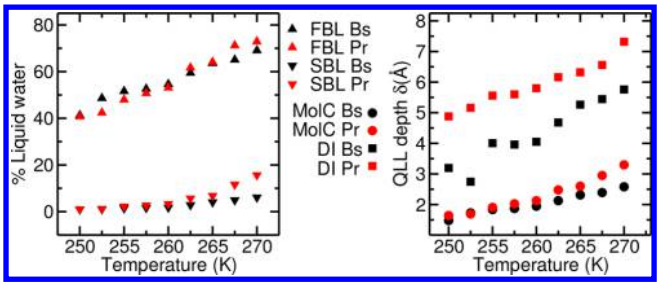

Figure 7. Left panel: percentage of liquid water in the first (FBL) and second (SBL) outermost bilayers. Right panel: QLL thickness estimated with the MolC and DI methods. Bs and Pr stand for the basal and prismatic faces.

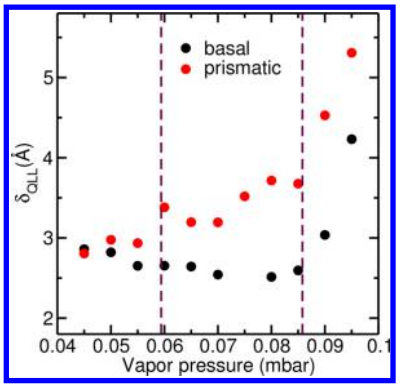

Figure 8. δ_{QLL} around the equilibrium vapor pressure at 270 K. The values are obtained with the MolC method. The vertical break lines corresponds to ±10% around the uncertainty of equilibrium vapor pressure.

use of the MolC approach results in smaller lengths, because it assumes a homogeneous phase and considers that the QLL consists only of liquid molecules, ignoring the solid ice present in the external layers, which does contribute to the total QLL extension when the DI method is applied. Moreover, the MolC measurement assigns approximately the same QLL width to both faces, because their corresponding liquid contents are almost identical. A difference in %LW arises in the second layer when approaching 270 K, where the amount of liquid water increases faster for the prismatic face: this directly redounds in a difference in the estimated values of δ_{QLL} around that temperature.

On the other hand, the MolC definition offers the advantage of providing instantaneous values for the thickness, since it only depends on the amount of liquid of a given configuration. This is not the case for the DI method, which, being based on the density profiles, yields δ_{QLL} values resulting from temporal averages. Hence, only the MolC method is appropriate to characterize δ_{QLL} in the kind of out of equilibrium GCMD simulations discussed below, where the utilization of an average density profile would be meaningless because condensation or evaporation can produce a time-dependent variation in the QLL thickness.

Advantages of the *μVT* Ensemble. According to Table 2, the description of the QLL is essentially equivalent in the three ensembles, when the system is in equilibrium conditions. Nevertheless, the μVT framework offers the possibility of mimicking experimental situations more properly than the other ensembles, since experiments are usually performed at a fixed vapor pressure. A precise control of this parameter, however, depends very much on the particular experimental setup, and so in many cases δ_{QLL} measurements are inevitably conducted slightly out of equilibrium. In this section we examine the QLL in understaturation and oversaturation conditions. The values for δ_{QLL} were obtained according to the MolC recipe, from GCMD simulations in the small cell at 270 K.

Figure 8 presents the thickness of the QLL as a function of P_v around the equilibrium value of 0.072 mbar. It can be seen that above the confidence interval for the equilibrium pressure, the average QLL depth increases noticeably. This behavior can be rationalized in terms of the solid−vapor equilibrium analyzed at the beginning of this section. When the chemical potential is above the saturation point, molecules tend to condense more quickly than the characteristic crystallization time, thus enlarging the QLL thickness. On the other hand, when working below saturation conditions, a QLL depth close to the equilibrium value is observed, which indicates that particle loss in an undersaturated atmosphere is accompanied by an almost simultaneous melting of the ice layer below, and a receding interface. We point out that, in this kind of Monte Carlo simulation, the dynamics tend to be accelerated with respect to the physical time; the deposition rate should then be faster than the experimental one, so the enlargement of the QLL at oversaturation conditions may not be necessarily seen in experiments. Nevertheless, since the evaporation rate is also enhanced, it is likely that the phenomenon observed below for undersaturation conditions, where evaporation is immediately followed by melting, be indeed present in laboratory measurements. Hence, this result suggests that the pressure should be controlled in experiments with a precision of at least 10% or that it should be kept slightly below the saturation point, where the QLL depth would not be significantly affected.

In particular, experimental methods based on the physical contact between the instrument and the sample may lead to the overestimation of the QLL thickness, as it is the case in AFM indentation measurements because of condensation between the interface and the tip. In this kind of experiment, force versus distance curves are analyzed in order to retrieve the QLL depth from the attractive part of the AFM force curve[2,11] ("jump in distance"). Grand canonical simulations can capture certain aspects of this process that may not be evident in the other ensembles. Thus, we performed preliminary *μVT* simulations including a hydrophilic sphere that represents an AFM tip over a slab exposing the basal face, in a box of dimensions 10.5 × 12.2 × 6.1 nm^3 plus 11.4 nm of vacuum. The probe, with a radius of 1.45 nm, was immobilized at a fixed distance from the surface by a harmonic potential. The interaction of the tip particles with water was the same as that of water with itself, thus behaving similarly to an hydrophilic silica surface.[30] These simulations were carried out at 270 K, fixing the chemical potential at the equilibrium value for that temperature. This kind of structural model has been proposed by Gelman and collaborators to reproduce the distance−force AFM curves with atomistic potentials in the NVT ensemble.[11,22]

Figure 9 presents two images corresponding to these simulations, where the tip is suspended at 8 and 7 Å from the surface. It can be seen that capillary condensation occurs between the tip and the basal surface, producing the growth of the liquid layer, and thus leading to an apparent increase in its thickness. As a matter of fact, the use of this tip would yield a significantly overestimated value of around 1.3 nm for δ_{QLL},

DOI: 10.1021/acs.jpcb.8b00784
J. Phys. Chem. B XXXX, XXX, XXX−XXX

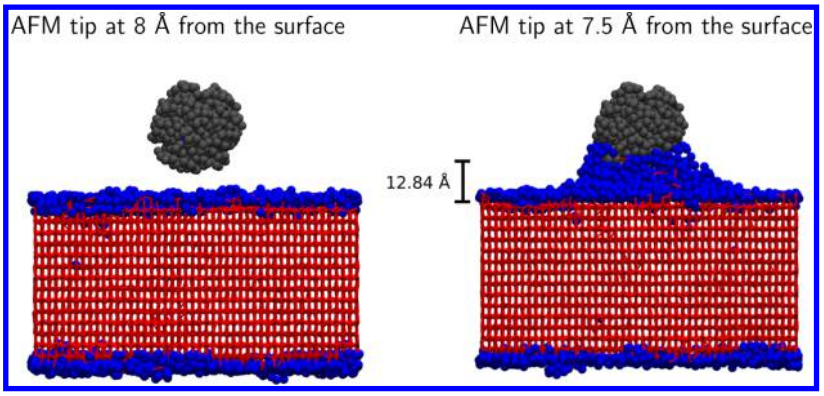

Figure 9. AFM probes represented with gray particles, placed 8 (left) and 7.5 Å (right) away from the surface. Liquid water molecules, shown in blue, condense between the probe and the ice surface, reaching an extension of 12.8 Å. The solid water is displayed with red sticks.

more than twice the value of the bare surface. This condensation phenomena might in part reconcile the discrepancies between simulations and experiments.

CONCLUDING REMARKS

We have studied the solid−vapor equilibrium for the Ih phase exposing the basal or the primary prismatic planes, employing the monatomic mW model. The solid−vapor equilibrium curve, recovered from constant chemical potential simulations, obeys the Clapeyron−Clausius relation and gives an enthalpy of sublimation of 50 kJ/mol for both faces, comparing very well with the experimental value of 51 kJ/mol.[39] An examination of the deposition dynamics showed that, on the basal face of Ih, the crystallization of cubic ice between layers forms stacking-disordered ice. The obtained sublimation enthalpy is in excellent agreement with the value reported by Molinero et al., computed from the difference between the enthalpy of the solid and that of a monatomic ideal gas, which turns out to be 1.7% lower than the experimental value at 273 K.[23] The similarity between the two computed enthalpies is remarkable in view of these totally different methodologies.

According to our analysis, and in agreement with recent results,[20] the outermost layers conforming the QLL are composed of two types of water molecules, belonging to a solid or to a liquid environment. The liquid and solid phases coexist in these layers in the form of nanophases, where clusters of solid H_2O of a few nanometers length are in equilibrium with regions of liquid. The liquid phase has a significant presence in the outermost layer and is distributed over its entire width, even at 250 K, suggesting that the picture of a QLL of a well-defined depth misses some important information. Describing the QLL in terms of the proportion of solid to liquid, and the distribution of liquid through the bilayers, might be more appropriate to characterize the interfacial structure. To test this view of the QLL phenomena, effort should be made in rationalizing the physical properties of these layers as the combination of molecules in a mixed solid and liquid environment. This viewpoint is in line with the recent SFG spectroscopy results for the basal face of ice Ih reported by Sanchez et al.[9] We quote from their work: "the spectra between 235 and 269 K can be very well described by a linear combination of the spectra at 235 and 269 K". This result gives strength to our interpretation of the nature of the outermost layers of the slab, as water molecules forming part of a nanosegregated solid and liquid system, in accordance with their observation of a layer by layer melt.

The description of the ice surface provided in the present study has been recently anticipated by Hudait, Allen and Molinero, who, based also on the mW model and the CHILL+ algorithm reported for the basal face at 260 K that 38% of water is melted.[20] The slight quantitative discrepancy, we determined a 50% of liquid at that temperature, might be attributed to the criterion adopted to select the molecules taking part of the QLL: whereas Hudait and coauthors count the liquid molecules in a fringe of 12 Å from the vapor interface, our value considers exclusively the particles in the outermost layer. The inclusion of molecules lying underneath would lead to a decrease in the amount of liquid. In the present work we have expanded the analysis to different temperatures and ensembles taking special care to identify the nature of water layer by layer. In our simulations, liquid water does not significantly appear in the second layer until a certain percentage of liquid is reached in the outermost one. At 250 K, with an approximate content of 40% of liquid in the external interface for both basal and prismatic planes, there is a negligible amount of liquid water in the second bilayer. At 270 K, though, with a 70% of liquid in the most external layer, the percentage in the second bilayer raises to 6% for the basal and 15% for the primary prismatic faces.

The QLL thicknesses found in this work using both the MolC and DI methods are in the order of a few angstroms, in agreement with the values reported in other simulations. The DI method provides a larger QLL depth because it takes into account the actual distribution of the liquid phase in the bilayer and the intrinsic bilayer width, giving a result that follows the trend of the water percentage at the interface. We observed for the mW model that, close to the melting temperature, the QLL on the basal face is slightly thinner than on the primary prismatic surface, which is opposite to what have been found for the TIP4P/ice force-field by Conde and co-workers[16] but in accordance with the results of Gelman et al. for the TIP4P-EW model.[22] This shows that the differences in QLL depths between the faces of ice Ih obtained computationally are subtle and model dependent.

The QLL thicknesses obtained in the present simulations turn out to be at least 1 order of magnitude lower than most experimental results. They do not exhibit a clear dependence with either the size of the exposed surface or the simulation ensemble, however, the μVT ensemble involves some advantages that must be highlighted. One of this is the possibility of assigning the error in the QLL depth, or in %LW, according to the uncertainty in the vapor pressure, which can

DOI: 10.1021/acs.jpcb.8b00784
J. Phys. Chem. B XXXX, XXX, XXX−XXX

be related to experimental conditions, where the control of the vapor pressure is of key importance to study the QLL at equilibrium. We have corroborated this last statement when performing μVT simulations out of equilibrium, showing that 10% above the confidence interval of the equilibrium pressure, it is possible to find significant differences in the QLL depth.

The μVT ensemble also offers the possibility of mimicking the condensation induced by an external probe, allowing for a molecular interpretation of the experimental data. This has been illustrated in our preliminary example of capillary condensation in an AFM tip, which enlarges the apparent QLL layer by a factor of 2 or more. Moreover, GCMD simulations might be of help to clarify some of the differences often observed between simulation and experiments. For example, in the experimental work by Sazaki et al.,[6] the QLL depth of the basal face was analyzed with a state of the art optical technique that combines laser confocal microscopy with differential interference contrast microscopy (LCM-DIM). This technique, which in principle allows for an average resolution of 5 Å normal to the surface, and a lateral resolution of the order of micrometers, revealed the existence of two phases of QLL named α and β. The α-QLL phase has a geometry of liquid water droplets with very small contact angle above the solid surface, having a height of the order of hundreds of nanometers and a width of tens of micrometers. The β-QLL phase has a laminar morphology, but its height is below the quantification limit of the technique. The same group interpreted this observation as an out of equilibrium phenomenon,[40] meaning that formation of these structures are only observed above or below the equilibrium vapor pressure. It would be of great importance to corroborate this last statement with grand canonical molecular simulations. Yet, it must be noted that simulation boxes of tens of nanometers would be necessary to approach a fraction of the scale of the experiment. In any case, the question is worth exploring because it could shed light on whether the QLL described by the simulations is of a different origin than the one observed in experiments. This might be another reason for the discrepancy in the QLL depths.

AUTHOR INFORMATION

Corresponding Author

*E-mail: mfactorovich@qi.fcen.uba.ar.

ORCID

Damian A. Scherlis: 0000-0002-0588-287X

Matías H. Factorovich: 0000-0001-5611-8751

Present Address

[§]Theoretische Chemie Institut für Physikalische Chemie, Georg-August-Universität Göttingen, Tammannstr. 6, D-37077 Göttingen, Germany.

Notes

The authors declare no competing financial interest.

ACKNOWLEDGMENTS

We would like to thank Julian Gelman Constantin for having introduced us to this subject and for his support in the preparation of the initial model systems. This study has been funded by grants of ANPCYT/PICT 2012-2292 and UBACYT 20020160100124BA. We thank the Center of High Performance Computing of the University of Utah for an award of computing time and technical support in the framework of a collaboration with the group of Valeria Molinero.

REFERENCES

(1) Dosch, H.; Lied, A.; Bilgram, J. Glancing-angle X-ray scattering studies of the premelting of ice surfaces. *Surf. Sci.* **1995**, *327*, 145−164.

(2) Döppenschmidt, A.; Butt, H.-J. Measuring the thickness of the liquid-like layer on ice surfaces with atomic force microscopy. *Langmuir* **2000**, *16*, 6709−6714.

(3) Golecki, I.; Jaccard, C. Intrinsic surface disorder in ice near the melting point. *J. Phys. C: Solid State Phys.* **1978**, *11*, 4229−4237.

(4) Furukawa, Y.; Yamamoto, M.; Kuroda, T. Ellipsometric study of the transition layer on the surface of an ice crystal. *J. Cryst. Growth* **1987**, *82*, 665−677.

(5) Elbaum, M.; Lipson, S.; Dash, J. Optical study of surface melting on ice. *J. Cryst. Growth* **1993**, *129*, 491−505.

(6) Sazaki, G.; Zepeda, S.; Nakatsubo, S.; Yokomine, M.; Furukawa, Y. Quasi-liquid layers on ice crystal surfaces are made up of two different phases. *Proc. Natl. Acad. Sci. U. S. A.* **2012**, *109*, 1052−1055.

(7) Sadtchenko, V.; Ewing, G. Interfacial melting of thin ice films: An infrared study. *J. Chem. Phys.* **2002**, *116*, 4686−4697.

(8) Bluhm, H.; Ogletree, D.; Fadley, C.; Hussain, Z.; Salmeron, M. The premelting of ice studied with photoelectron spectroscopy. *J. Phys.: Condens. Matter* **2002**, *14*, L227−L233.

(9) Sánchez, M. A.; et al. Experimental and theoretical evidence for bilayer-by-bilayer surface melting of crystalline ice. *Proc. Natl. Acad. Sci. U. S. A.* **2017**, *114*, 227−232.

(10) Björneholm, O.; Hansen, M.; Hodgson, A.; Liu, L.-M.; Limmer, D.; Michaelides, A.; Pedevilla, P.; Rossmeisl, J.; Shen, H.; Tocci, G.; Tyrode, E.; et al. Water at Interfaces. *Chem. Rev.* **2016**, *116*, 7698−7726.

(11) Constantin, J. G. Propiedades termodinámicas y estructurales de nanoagregados de agua y de la interfase hielo-aire. Ph.D. Thesis; Universidad de Buenos Aires: Buenos Aires, Argentina, 2015.

(12) Henson, B. F.; Voss, L. F.; Wilson, K. R.; Robinson, J. M. Thermodynamic model of quasiliquid formation on H2O ice: Comparison with experiment. *J. Chem. Phys.* **2005**, *123*, 144707.

(13) Murray, B. J.; Bertram, A. K. Formation and stability of cubic ice in water droplets. *Phys. Chem. Chem. Phys.* **2006**, *8*, 186−192.

(14) Franks, F. *Water, a Comprehensive Treatise: The physics and physical chemistry of water*; Water, a Comprehensive Treatise v. 1; v. 7; Plenum Press: New York, 1972; Chapter 4.

(15) Kroes, G.-J. Surface melting of the (0001) face of TIP4P ice. *Surf. Sci.* **1992**, *275*, 365−382.

(16) Conde, M. M.; Vega, C.; Patrykiejew, A. The thickness of a liquid layer on the free surface of ice as obtained from computer simulation. *J. Chem. Phys.* **2008**, *129*, 014702.

(17) Paesani, F.; Voth, G. A. Quantum effects strongly influence the surface premelting of ice. *J. Phys. Chem. C* **2008**, *112*, 324−327.

(18) Limmer, D. T.; Chandler, D. Premelting, fluctuations, and coarse-graining of water-ice interfaces. *J. Chem. Phys.* **2014**, *141*, 18C505.

(19) Shepherd, T. D.; Koc, M. A.; Molinero, V. The Quasi-Liquid Layer of ice under conditions of Methane clathrate formation. *J. Phys. Chem. C* **2012**, *116*, 12172−12180.

(20) Hudait, A.; Allen, M. T.; Molinero, V. Sink or Swim: ions and organics at the IceAir interface. *J. Am. Chem. Soc.* **2017**, *139*, 10095−10103.

(21) Nguyen, A. H.; Molinero, V. Identification of clathrate hydrates, hexagonal ice, cubic ice, and liquid water in simulations: the CHILL+ algorithm. *J. Phys. Chem. B* **2015**, *119*, 9369−9376.

(22) Gelman Constantin, J.; Carignano, M. A.; Corti, H. R.; Szleifer, I. Molecular dynamics simulation of ice indentation by model atomic force microscopy tips. *J. Phys. Chem. C* **2015**, *119*, 27118−27124.

(23) Molinero, V.; Moore, E. B. Water modeled as an intermediate element between carbon and silicon. *J. Phys. Chem. B* **2009**, *113*, 4008−4016.

(24) Hudait, A.; Molinero, V. What determines the ice polymorph in clouds? *J. Am. Chem. Soc.* **2016**, *138*, 8958−8967.

(25) Lupi, L.; Molinero, V. Does hydrophilicity of carbon particles improve their ice nucleation ability? *J. Phys. Chem. A* **2014**, *118*, 7330−7337.

DOI: 10.1021/acs.jpcb.8b00784
J. Phys. Chem. B XXXX, XXX, XXX−XXX

(26) Hudait, A.; Qiu, S.; Lupi, L.; Molinero, V. Free energy contributions and structural characterization of stacking disordered ices. *Phys. Chem. Chem. Phys.* **2016**, *18*, 9544−9553.
(27) Perez Sirkin, Y.; Factorovich, M.; Molinero, V.; Scherlis, D. Vapor pressure of aqueous solutions of electrolytes reproduced with coarse-grained models without electrostatics. *J. Chem. Theory Comput.* **2016**, *12*, 2942−2949.
(28) Factorovich, M.; Molinero, V.; Scherlis, D. A simple grand canonical approach to compute the vapor pressure of bulk and finite size systems. *J. Chem. Phys.* **2014**, *140*, 064111.
(29) Factorovich, M.; Molinero, V.; Scherlis, D. Vapor pressure of water nanodroplets. *J. Am. Chem. Soc.* **2014**, *136*, 4508−4514.
(30) Factorovich, M. H.; Gonzalez Solveyra, E.; Molinero, V.; Scherlis, D. A. Sorption isotherms of water in nanopores: relationship between hydropohobicity, adsorption pressure, and hysteresis. *J. Phys. Chem. C* **2014**, *118*, 16290−16300.
(31) Stillinger, F. H.; Weber, T. A. Computer simulation of local order in condensed phases of silicon. *Phys. Rev. B: Condens. Matter Mater. Phys.* **1985**, *31*, 5262−5271.
(32) Perez Sirkin, Y. A.; Factorovich, M. H.; Molinero, V.; Scherlis, D. A. Stability and vapor pressure of aqueous aggregates and aerosols containing a monovalent ion. *J. Phys. Chem. A* **2017**, *121*, 2597−2602.
(33) Plimpton, S. Fast parallel algorithms for short-Range molecular dynamics. *J. Comput. Phys.* **1995**, *117*, 1−19.
(34) Kroll, D. M.; Lipowsky, R. Interface delocalization transitions in semi-infinite systems. *Phys. Rev. B: Condens. Matter Mater. Phys.* **1983**, *28*, 6435−6442.
(35) Nada, H.; Furukawa, Y. Anisotropy in growth kinetics at interfaces between proton-disordered hexagonal ice and water: a molecular dynamics study using the six-site model of {H2O}. *J. Cryst. Growth* **2005**, *283*, 242−256.
(36) Malkin, T. L.; Murray, B. J.; Salzmann, C. G.; Molinero, V.; Pickering, S. J.; Whale, T. F. Stacking disorder in ice I. *Phys. Chem. Chem. Phys.* **2015**, *17*, 60−76.
(37) Hudait, A.; Molinero, V. Ice Crystallization in Ultrafine Water-Salt Aerosols: Nucleation, Ice-Solution Equilibrium, and Internal Structure. *J. Am. Chem. Soc.* **2014**, *136*, 8081−8093.
(38) Lu, J.; Chakravarty, C.; Molinero, V. Relationship between the line of density anomaly and the lines of melting, crystallization, cavitation, and liquid spinodal in coarse-grained water models. *J. Chem. Phys.* **2016**, *144*, 234507.
(39) Feistel, R.; Wagner, W. A new equation of state for H2O ice Ih. *J. Phys. Chem. Ref. Data* **2006**, *35*, 1021−1047.
(40) Murata, K.-i.; Asakawa, H.; Nagashima, K.; Furukawa, Y.; Sazaki, G. Thermodynamic origin of surface melting on ice crystals. *Proc. Natl. Acad. Sci. U. S. A.* **2016**, *113*, E6741−E6748.

DOI: 10.1021/acs.jpcb.8b00784
J. Phys. Chem. B XXXX, XXX, XXX−XXX